JOC The Journal of Organic Chemistry
Cite This: J. Org. Chem. 2020, 85, 129−141
Article
pubs.acs.org/joc

Precision Nanotube Mimics via Self-Assembly of Programmed Carbon Nanohoops

Jeff M. Van Raden,[†,∥] Erik J. Leonhardt,[†,∥] Lev N. Zakharov,[‡] A. Pérez-Guardiola,[§] A. J. Pérez-Jiménez,[§] Checkers R. Marshall,[†] Carl K. Brozek,[†] J. C. Sancho-García,*[,§] and Ramesh Jasti*[,†,∥]

[†]Department of Chemistry & Biochemistry and Materials Science Institute, University of Oregon, Eugene, Oregon 97403, United States

[∥]Knight Campus for Accelerating Scientific Impact, University of Oregon, Eugene, Oregon 97403, United States

[‡]CAMCOR − Center for Advanced Materials Characterization in Oregon, University of Oregon, Eugene, Oregon 97403, United States

[§]Department of Physical Chemistry, University of Alicante, E-03080 Alicante, Spain

Supporting Information

ABSTRACT: The scalable production of homogeneous, uniform carbon nanomaterials represents a key synthetic challenge for contemporary organic synthesis as nearly all current fabrication methods provide heterogeneous mixtures of various carbonized products. For carbon nanotubes (CNTs) in particular, the inability to access structures with specific diameters or chiralities severely limits their potential applications. Here, we present a general approach to access solid-state CNT mimic structures via the self-assembly of fluorinated nanohoops, which can be synthesized in a scalable, size-selective fashion. X-ray crystallography reveals that these CNT mimics exhibit uniform channel diameters that are precisely defined by the diameter of their nanohoop constituents, which self-assemble in a tubular fashion via a combination of arene-pefluoroarene and C−H—F interactions. The nanotube-like assembly of these systems results in capabilities such as linear guest alignment and accessible channels, both of which are observed in CNTs but not in the analogous all-hydrocarbon nanohoop systems. Calculations suggest that the organofluorine interactions observed in the crystal structure are indeed critical in the self-assembly and robustness of the CNT mimic systems. This work establishes the self-assembly of carbon nanohoops via weak interactions as an attractive means to generate solid-state materials that mimic carbon nanotubes, importantly with the unparalleled tunability enabled by organic synthesis.

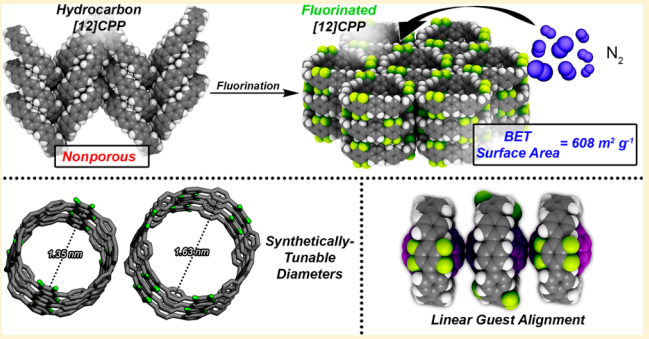

INTRODUCTION

The remarkable properties of carbon nanomaterials continue to drive fundamental and applied research advancements across a multitude of fields.[1−3] Recently, the nanoscale confinement and smooth molecular topology afforded by materials such as carbon nanotubes (CNTs) and graphene have proven indispensable in the emerging area of nanofluidics,[4−7] promising revolutionary applications in water desalination and biomimetic channel construction. Carbon nanomaterials, however, are difficult to synthesize in a uniform, homogeneous manner, with most modern fabrication methods affording ill-defined heterogeneous mixtures of carbonized products. As a result of these limitations, a CNT of a particular diameter and chirality, for example, cannot be accessed directly. This is problematic as both CNT diameter and chirality dictate the observed behavior and thus the utility of the material.[1] The ability to control carbon connectivity within carbon nanomaterials with atom-level precision would therefore be broadly impactful as their materials properties could be finely tuned to meet specific applications, which would undoubtedly accelerate discoveries within the field.

By perfecting a balance between covalent and noncovalent interactions, nature has developed a powerful design strategy to construct highly complex, yet well-defined nanoarchitectures. This is perhaps best illustrated in molecular biology where covalently linked "programmed" small molecule building blocks engage in numerous secondary noncovalent interactions, ultimately giving rise to high functioning biological machinery.[8] Thus, as a guide, nature has provided synthetic

Special Issue: Functional Organic Materials

Received: August 28, 2019
Published: October 18, 2019

DOI: 10.1021/acs.joc.9b02340
J. Org. Chem. 2020, 85, 129−141

chemists with important blueprints for developing new materials, a factor that has contributed to the development of homogeneous, well-defined materials such as metal−organic frameworks (MOFs)[9,10] and covalent-organic frameworks (COFs).[11,12] A key design feature is the inclusion of reversible, noncovalent interactions, which provides a pathway to structural homogeneity while requiring relatively little energy in contrast to current methods for traditional carbon nanomaterial synthesis. Inspired by these principles, we envisioned a noncovalent approach to the synthesis of well-defined CNT mimics, where key features such as diameter and chirality are programmed via simple small molecule building blocks. While self-assembled nanotube-like architectures are well-known,[13−15] those that successfully replicate the fully conjugated radial geometry of CNTs—a key property that gives rise to many of the observed confinement effects—remain largely underexplored.

Since the initial synthesis of the cycloparaphenylenes in 2008,[16] macrocycles with radial geometry have become increasingly common due to the advancement of appropriate strain-building synthetic methods.[17−22] Considering their structural relationship to CNTs, we envisioned that these relatively new macrocyclic structures could act as the desired small-molecule building blocks for self-assembled CNT-like solid-state materials. These "carbon nanohoops", however, do not naturally crystallize into tubular structures in the solid state. Instead, these molecules tend to self-assemble into staggered, herringbone-like packing motifs to minimize the void space created by the rigid macrocyclic structure.[23,24] We hypothesized that with the appropriate secondary interactions, these "CNT fragments" could be programmed to arrange into columnar arrays, similar to that of CNTs. To this end, recently, we reported the synthesis of a fluorinated nanohoop, **1**, that, in the solid state, readily self-assembles into nanotube-like columns that closely mimic CNT channels (Figure 1).[25] Unlike traditional carbon nanomaterials, however, **1** is accessed via bottom-up organic synthesis, allowing for the diameter and connectivity of the self-assembled CNT mimics to be precisely defined. Through X-ray crystallographic analysis, we posited that this self-assembly arises from a combination of arene-perfluoroarene[26] and C−H—F[27] interactions. Moreover, we found it was possible to vertically assemble "forests" of these CNT mimics on graphite surfaces via mild solution casting, suggesting facile integration in a multitude of applications.

While fluorination successfully oriented the nanohoops into the desired CNT-like geometry, it was not clear the extent to which this self-assembly strategy could be regarded as a general strategy to CNT mimics. For example, in our initial report, we only examined the self-assembly of a single diameter nanohoop with a very specific fluorination pattern, raising the question of generality. Related to this, the underlying secondary interactions were not systematically investigated and therefore were not fully understood. We also recognized that in order for these materials to be considered genuine CNT mimics, these self-assembled systems would also have to exhibit some degree of CNT functionality. Accordingly, in this work, we expand on our previous report by demonstrating that these fluorinated, self-assembling nanohoops exhibit structural features and functions that have been previously observed in traditional CNTs, ultimately establishing fluorinated nanohoops as a new CNT-like precision nanomaterial. First, we describe the synthesis of two new fluorinated derivates—a reduced diameter [10]CPP analog and a [12]CPP derivative with a

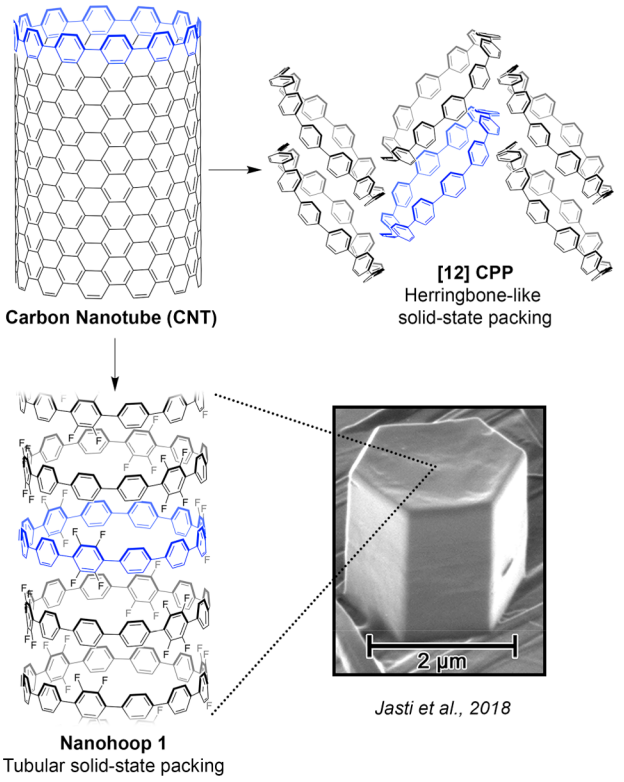

Figure 1. CNT fragment [12]CPP exhibits a herringbone-like packing in the solid state, while nanohoop **1**, a fluorinated CNT fragment, self-assembles into nanotube-like columns. These columns can be fabricated in vertical "forests" on graphite substrates via mild solution casting, taking the form of hexagonal pillars (inset - Reprinted from ref 25. Copyright 2018 American Chemical Society.).

lesser degree of fluorination, both of which assemble into the desired CNT mimic structures. Importantly, we illustrate the scalabilty of these materials through a new gram-scale synthesis of previously reported nanohoop **1**. Next, we show that the [10]CPP analog is capable of linearly aligning C_{60} molecules as observed in CNT@C_{60} peapod structures and that **1** shows microporosity at 77 K via N_2 uptake measurements. Neither of the above functionalities are observed in the respective nonfluorinated analogs, supporting our hypothesis that fluorination of the nanohoop backbone is an effective general strategy toward fabricating robust CNT solid-state mimics. Finally, a theoretical analysis of the CNT mimic systems is presented which supports our hypothesis that weak organo-fluorine interactions drive the self-assembly of the fluorinated nanohoop constituents. Moreover, the computational methods described here provide a predictive tool for the design of future solid-state CNT mimics.

RESULTS AND DISCUSSION

Synthesis and X-ray Crystal Structure Analysis. A primary aim of this study was to determine if the supramolecular design strategy we had employed with nanohoop **1** was amenable to nanohoops of varying diameter and fluorination patterns. Additionally, we sought to develop a modular synthetic strategy where access to fluorinated structures of differing diameter and fluorination patterns could be quickly obtained via common intermediates. Another key focus point was to improve the overall reaction efficiency over the low yielding synthetic route we had previously used to

DOI: 10.1021/acs.joc.9b02340
J. Org. Chem. 2020, 85, 129−141

Scheme 1. Synthetic Routes Towards Nanohoops 2, 3, and 1

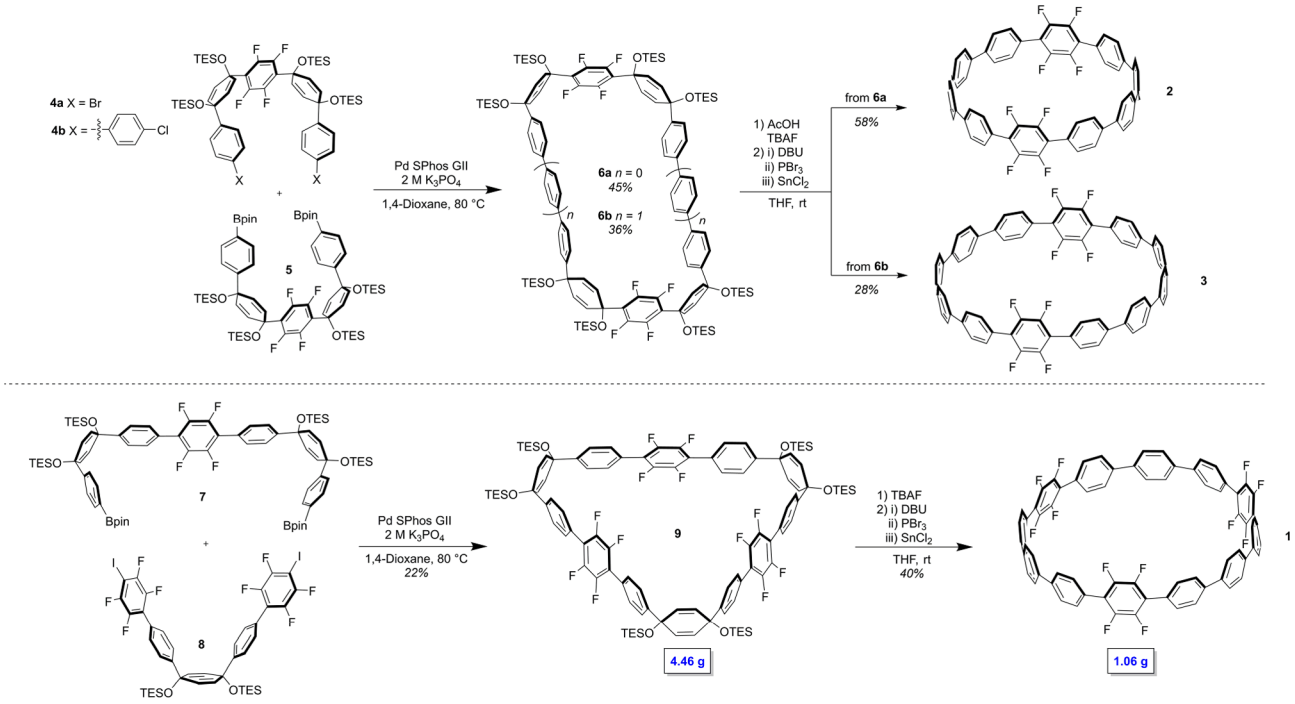

access **1**—a severe limitation that ultimately hindered our ability to explore the solid-state materials properties of **1**. Ultimately, we aimed to synthesize nanohoops **2** (a [10]CPP analog) and **3** (a [12]CPP analog), which each bear two symmetrically placed tetrafluorophenylene moieties. Critical to our investigation was the acquisition of single crystals of **2** and **3** suitable for X-ray diffraction in order to unambiguously determine the solid state packing of these materials and also to allow for the detailed analysis of arene-perfluoroarene and C−H—F interactions present in the solid-state arrangements.

With this in mind, we proceeded toward both **2** and **3** via our previously reported curved building blocks **4a**, **4b**, and **5**.[25] Importantly, each of these intermediates can be prepared on a multigram scale in excellent yield. Under dilute Suzuki-Miyaura cross-coupling conditions, triethylsilyl (TES) protected macrocycles **6a** and **6b** were synthesized in modest yields (Scheme 1). To overcome the highly strained nature of nanohoops and their derivatives, macrocyclic intermediates such as **6a** and **6b** are often prepared, where the embedded cyclohexadiene fragments act as "masked" benzene units.[17,19] Typically, after cleavage of the silyl protecting groups, the cyclohexadiene units can undergo reductive aromatization to give the final fully conjugated nanohoop.[19] In this case, however, we found that treatment of macrocycles **6a** and **6b** with tetrabutylammonium fluoride (TBAF) consistently resulted in decomposition. We reasoned that the electron-withdrawing nature of the fluorinated aryl rings can promote a retroaddition reaction, ultimately resulting in a cyclohexadienone and an unstable anionic tetrafluoraryl ring. After screening various conditions, we found that the addition of excess acetic acid to the reaction mixture allowed for clean conversion to the desired free-alcohol functionalized macrocycles. However, as reported by both the Yamago group[28] and our lab,[25] reductive aromatization with H_2SnCl_4 led to the desired products in low yield (15% and 12% for **2** and **3**, respectively). Through slight modification of the conditions reported by Yamago and co-workers,[28,29] we were able to improve the yield of both **2** (58% yield) and **3** (28% yield), providing ample material for our ongoing investigations.

Encouraged by this improvement, we then applied these optimized aromatization conditions to our original synthesis of nanohoop **1**. Unfortunately, we found that subjecting our previously reported cyclohexadiene-based macrocycle to these conditions gave a complex, insoluble mixture. With the hypothesis that fluorinated aryl rings adjacent to the cyclohexadiene may still undergo an undesired macrocyclic ring-opening type reaction, we developed a new synthetic route using "C" shaped intermediate **7** and previously reported "V" shaped intermediate **8**. In this case, macrocycle **9**, which does not contain fluorinated aryl rings adjacent to cyclohexadienes, smoothly undergoes reductive aromatization to produce **1** on gram scale. Given that we have already demonstrated the potential utility of **1** as a new, flexible optoelectronic nanomaterial, this improved synthetic route will accelerate further studies of its solid-state properties.

As previously reported,[25] nanohoop **1** self-assembles into perfectly linear nanotube-like arrays in the solid state, forming channels that are precisely 1.63 nm in diameter (Figure 2a). The 3-fold symmetry of the molecule allows for six arene-perfluoroarene interactions per hoop, each of which measures at 3.68 Å (Figure 2b).[31,32] This results in an ideal hexagonal circle-packing motif, which is the densest theoretical packing possible for circles of identical diameter.[30] Vertical assembly in the solid-state architecture of **1** is guided by 18 C−H—F interactions per hoop dimer (Figure 2c), which range in distance from 2.53−2.62 Å (for completeness, C−F distances are also included for each crystal structure in Figure 2).[27] The readily apparent organofluorine interactions observed in the crystal packing of **1** provide an excellent reference point when analyzing the X-ray crystal structures of **2** and **3**.

Following the synthesis of nanohoop **2**, needlelike single-crystals suitable for X-ray crystallography were obtained by

DOI: 10.1021/acs.joc.9b02340
J. Org. Chem. 2020, 85, 129−141

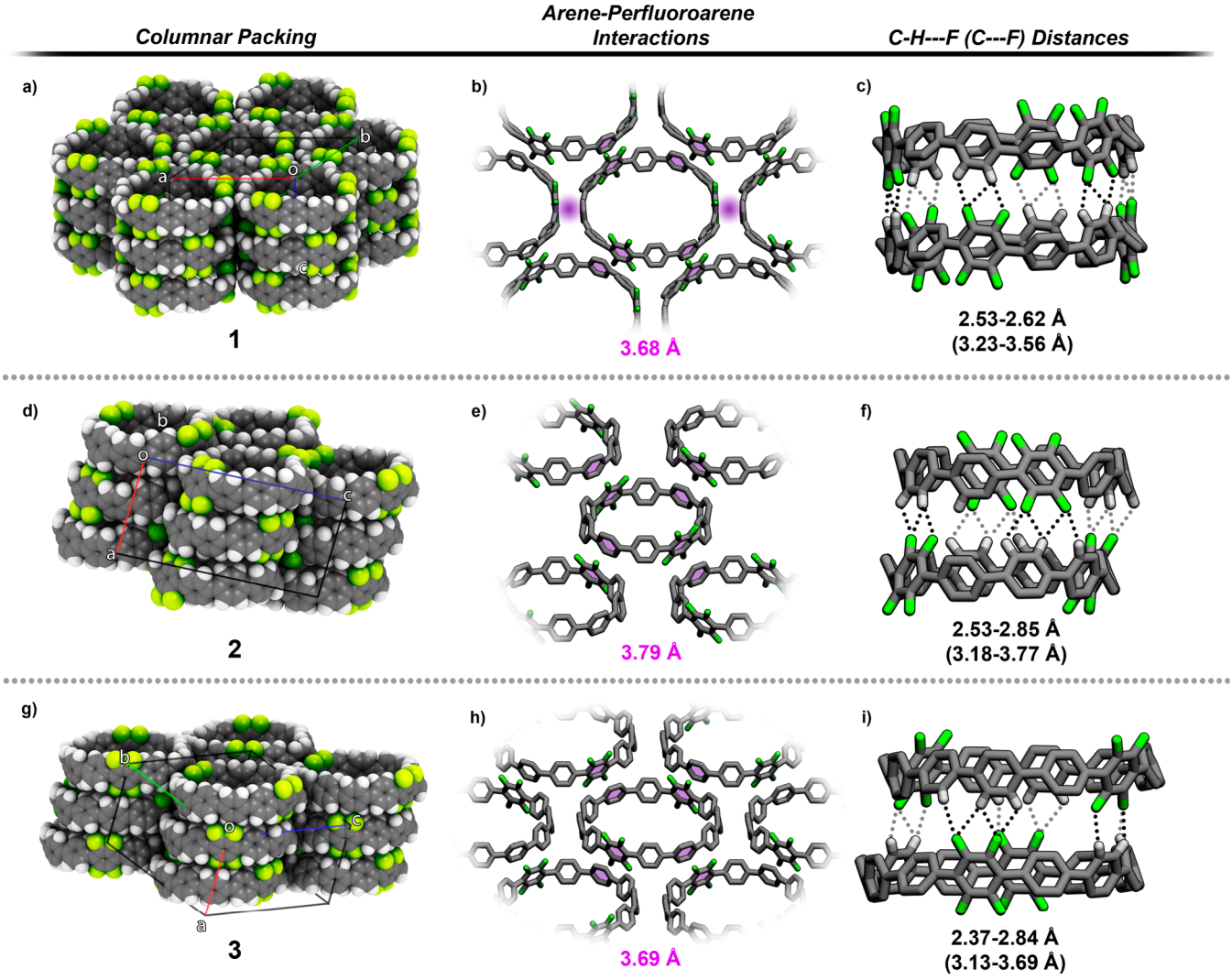

Figure 2. Columnar packing, arene-perfluoroarene interactions (highlighted in purple), and C−H—F distances (dotted lines, C−F distances shown in parentheses) observed in the crystal packings of nanohoops **1** (a-c), **2** (d-f), and **3** (g-i).

slow evaporation of a THF solution of fluorinated nanohoop **2**. The solid-state packing of **2** affords staggered nanotube-like columns (Figure 2d) with channel diameters of precisely 1.38 nm. As was observed previously for **1**, the horizontal arrangement of **2** was found to be guided by arene-perfluoroarene interactions. Four of these interactions can be found in the crystal structure of **2**, all measuring at 3.78 Å (Figure 2e). Likewise, the vertical alignment of **2** in the solid state is dictated by a multitude of C−H—F interactions, as was also the case with **1**. A total of 16 C−H—F interactions were observed, measuring between 2.53−2.85 Å (Figure 2f). It should be stressed that the packing of **2** is significantly different than that of parent [10]CPP,[33,34] which adopts a herringbone-type motif—a common observation in the all-hydrocarbon parent nanohoops.

Slow evaporation of **3** in dichloromethane (DCM) afforded needlelike crystals similar in appearance to those formed by **1** and **2**. Single-crystal XRD analysis revealed that **3** also self-assembles into tubular arrays (Figure 2g), again in stark contrast to the herringbone-like packing of the all-hydrocarbon analog of [12]CPP. Upon closer inspection of the crystal structure of **3**, we observed four aryl-perfluoro aryl distances measuring at 3.69 Å (Figure 2h) and 13 C−H—F interactions ranging between 2.48 and 2.84 Å (Figure 2i). The solid-state packing of **3** in comparison to **1** is particularly interesting in that it shows how different tubular arrangements of nanohoops of identical size can be achieved through varying both the extent of fluorination in the nanohoop backbone and the symmetry of this fluorination.

While the 3-fold symmetry of **1** results in linear channels (Figure 3a) and an ideal hexagonal circle packing arrangement, the 2-fold symmetry of **3** affords staggered columns and a pseudohexagonal horizontal assembly. Also, due to the inclusion of only two tetrafluorophenylene moieties, **3** exhibits two fewer arene-perfluoroarene interactions and 23 fewer C−H—F interactions (Figures 2h and 2i) than found in the crystal structure of **1**. Thus, we predict that organofluorine interactions may also allow for the further construction of tubular nanohoop-based assemblies with slightly varied morphologies but identical diameters.

The crystal structure analyses in this work suggest that fluorination is a relatively predictable and reliable strategy for accessing nanotube-like systems via nanohoop self-assembly. However, it should be noted that the 2-fold symmetry found in **1** and **2** has been shown to result in nontubular arrangements in fluorinated nanohoop systems. Indeed, Yamago and co-

DOI: 10.1021/acs.joc.9b02340
J. Org. Chem. 2020, 85, 129−141

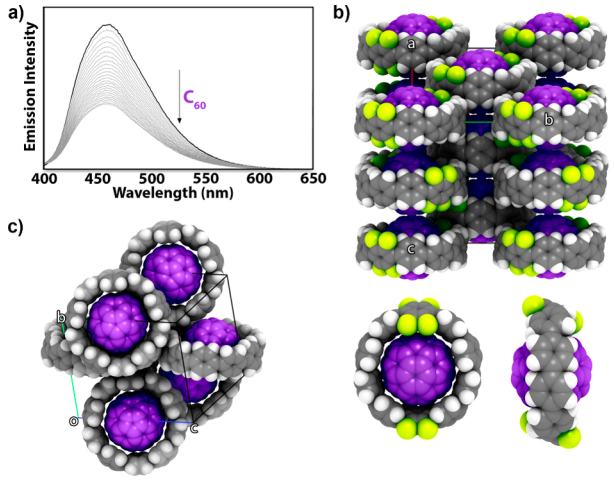

Figure 3. a) Observed emission response of nanohoop **2** to increasing quantities of C_{60}. b) Peapodlike crystal packing of the **2**@C_{60} complex (top) and views of a single host–guest complex (bottom); c) X-ray crystal structure of the [10]CPP@C_{60} complex in the solid state. Fluorine atoms are colored in green, hydrogens are colored in white, carbons are colored in gray, and C_{60} has been colored purple.

workers found that a 2-fold symmetric fluorinated [6]CPP analog exhibits herringbone-like packing, presumably since this staggered arrangement allows for the maximization of solid-state C–H—F interactions.[28] Likewise, the same study by Yamago provided an example of a 3-fold symmetric nanohoop (a [9]CPP analog) that assembles into tubular arrangements without the guidance of arene-perfluoroarene interactions, instead appearing to rely solely on C–H—F interactions. Therefore, we conclude that both nanohoop diameter and skeletal symmetry (i.e., the number of phenylene moieties present) are crucial factors to consider in the design of such systems.

Solid- and Solution-State Analysis of the C_{60}@2 Host–Guest Complex. A notable application of CNT channels is the uptake and confinement of small molecule guests into 1D channels.[35−37] Thus, we were curious if the nanotube-like channels formed by fluorinated nanohoops are accessible to guests. As an initial approach, we sought to leverage the size and shape complementarity of fluorinated nanohoop **2**, a [10]CPP derivative, with C_{60}.[34,38] Indeed, macrocycles with radially oriented π-conjugation,[39] in particular [10]CPP and its derivatives,[40,41] have been shown to be strong hosts for C_{60} in both solution and the solid state. Similar to the case of C_{60}@ [10]CPP, we found that the addition of C_{60} to fluorinated nanohoop **2** resulted in a decrease in the fluorescence intensity of fluorinated nanohoop **2** (Figure 3a). From these fluorescence quenching data, we determined a binding constant (K_a) of $8.1 \pm 0.2 \times 10^5$ L^{-1} mol between fluorinated nanohoop **2** and C_{60} (Figure S4), a value that is lower than most binding constants reported [10]CPP hosts. For example, as compared to the parent [10]CPP host, the K_a is reduced (C_{60}@[10]CPP complex = $2.71 \pm 0.03 \times 10^6$ L^{-1} mol)[38] by nearly 30%. Despite this lowered affinity, the value is still relatively high among various fullerene hosts—a factor that allowed for a detailed investigation into the solid-state chemistry between nanohoop **2** and C_{60}. Dark red single-crystals of the C_{60}@**2** complex suitable for X-ray crystallography were grown via vapor diffusion of diethyl ether into a dilute THF/1,2-dichlorobenzene/toluene (1:1:1) solution of fluorinated nanohoop **2** and C_{60} (1:1). Interestingly, crystal structure analysis revealed cylindrical packing (Figure 3b) but with the absence of perfluoroarene–arene interactions; however, numerous C–H—F interactions were found measuring from 2.54 to 2.87 Å (Figure S5). These interactions appear to be the driving force behind the linear arrangement of the C_{60}@**2** complex in the solid state, as the analogous all-hydrocarbon [10]CPP@C_{60} complex has been previously shown to adopt a staggered packing motif (Figure 3c).[34] The packing of **2**@C_{60} bears a striking aesthetic resemblance to CNT@C_{60} peapod structures, which have been shown to exhibit numerous exotic properties unique from bulk C_{60}. While not reported here, we expect that this arrangement can be adopted to align both endohedral[42,43] and exohedrally[41] functionalized fullerenes, a prospect that will likely result in new charge transport properties. Furthermore, given that the host–guest chemistry between nanohoops is just beginning to emerge, we anticipate that fluorinated nanohoops can potentially direct and preorganize other guest molecules into columnar 1D arrays in a highly size-selective manner leading to new strategies for applications such as templated polymerizations[44] and organic[45] electronic materials.

N_2 Uptake Studies on Nanohoop 1. Encouraged by the thermal stability of nanohoop **1** as evidenced by thermogravimetric analysis (Figure S12) and by the ability of the supramolecular assemblies of **1** to withstand the low-pressure conditions required for SEM measurements,[25] we sought to measure the material's surface area. Following evacuation to 2 μtorr at 125 °C, the N_2 uptake of **1** was collected at 77 K. The resulting data shown in Figure 4 reveal a Type 1 isotherm. At

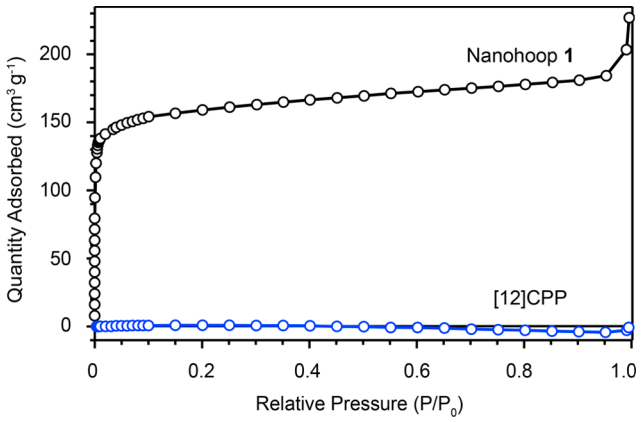

Figure 4. Comparison of N_2 uptake isotherms of **1** (black) and [12]CPP (blue) collected at 77 K.

low relative pressures P/P_0, high quantities of N_2 were adsorbed (Figure S13), indicating the presence of microporosity, i.e., pore diameters below 2 nm. Brunauer–Emmett–Teller (BET) analysis of these data produces a surface area of 608 m^2 g^{-1} (Figure S14). While this is a modest value in the general context of porous organic-based frameworks,[46−50] it is particularly high for an intrinsically porous system resulting from the assembly of macrocycles.[51−53] The calculated Saito-Foley cylindrical pore width of 0.74 nm for **1** is similar to the value reported previously for [12]CPP.[54] The crystallographic data, however, show an inner diameter of nanohoop **1** is 1.63 nm. The accuracy of the Saito-Foley equation is limited by assuming that pores are either completely full or empty and that the adsorbent packs perfectly.[55]

DOI: 10.1021/acs.joc.9b02340
J. Org. Chem. 2020, 85, 129−141

The related all-hydrocarbon [12]CPP exhibits little N_2 uptake when measured under the same conditions (Figure 4), which is consistent with our findings that the organofluorine interactions underlying the supramolecular assembly of **1** are strong and ordered. Although **1** and the nonfluorinated [12]CPP are similar in size, a measurable surface area will arise only if the nanohoop pores are easily accessible to adsorbate molecules. A previous study on [12]CPP also found that the pores were inaccessible to N_2 at 77 K, whereas measuring at 195 K showed substantially higher uptake.[54] Interestingly, this same report discovered that CO_2 adsorption at 195 K revealed a Type 1 isotherm that afforded a BET surface area of 503 $m^2 g^{-1}$. These observations suggested that the disordered assembly of [12]CPP prevented significant N_2 adsorption when rigidly fixed at low temperatures but permitted high uptake when allowed to reorient freely through thermally activated motion. While powder X-ray diffraction (PXRD) of [12]CPP after thermal activation has revealed it to be relatively disordered,[54] thermally activated **1** appears crystalline via PXRD. Interestingly, the activation process appears to actually induce ordering of the material, as PXRD measurements of a powder sample of **1** prior to heating and evacuation reveal a more amorphous character. We currently hypothesize that the observed crystallinity and microporosity of **1** after thermal activation can be attributed to the fluorination of the nanohoop backbone, as the all-hydrocarbon [12]CPP has been shown to be both amorphous and nonporous at 77 K after heating and evacuation. It is possible that, upon thermal activation, organofluorine interactions guide **1** into channels similar to those observed in the single crystal, which would then provide open pores for gas uptake.

Computational Analysis. To gain a more detailed understanding of the factors that govern and ultimately dictate the observed molecular packing arrangements, we turned to Density Functional Theorem (DFT). Given that fundamental properties such as molecular size and shape act in concert with intermolecular forces to give the most effective solid-state packing, an important consideration in gaining this understanding is to first determine the magnitude of interaction energy between neighboring molecules in the solid state. This is readily accomplished by first determining the interaction energy of nanohoop dimeric units from experimentally obtained solid-state data.[56] The intermolecular interaction energy of each unit (ΔE) is calculated by subtracting the monomer energies (at the observed dimer geometry) from that particular dimer. To account for both intra- and intermolecular noncovalent interactions, the D3(BJ) method[57,58] for dispersion-corrected DFT is applied, using the B3LYP functional[59] and the large cc-pVTZ basis set to avoid superposition errors. Calculations were carried out using the Gaussian 09 (D.01) package.[60]

To investigate this approach with fluorinated nanohoops, we opted to first investigate the forces involved in the solid-state molecular packing of **2**. As our design strategy relies on expected arene-perfluoroarene interactions, it would follow that fluorinated aryl rings of nanohoops such as **2** would possess a positive aromatic quadrupole moment (Qzz), similar to that observed in the case of hexafluorobenzene.[61] Indeed, the computationally determined Qzz for the fluorinated aryl rings of nanohoop **2** of were found to be 1.21×10^{-38} C m^2—a value of opposite sign for the model compound benzene ($Qzz = -29.2 \times 10^{-40}$ C m^2).[61] Additionally, when compared to 1,2,4,5-tetrafluorobenzene ($Qzz = 13.6 \times 10^{-40}$ C m^2),[62] the impact of the nanohoop framework is particularly apparent as the Qzz is considerably higher. Taken together, these findings highlight the underlying electronic structure involved in the observed solid-state arene-perfluoroarene interactions. Next, to understand energetic contributions of arene-perfluoroarene interactions in the crystal packing of **2**, we explored the various lateral interactions observed in the nanohoop's crystal structure, represented by the dimers in Figure 5. Importantly,

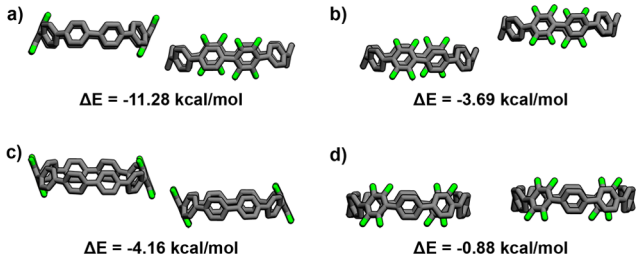

Figure 5. Set of lateral-like dimers extracted from the crystal structure of nanohoop **2** along with their respective interactions energies.

it was found that the dimer in which a tetrafluorophenylene ring of one nanohoop is aligned face-to-face with a nonfluorinated phenylene in the adjacent hoop (Figure 5a) exhibits a markedly high interaction energy ($\Delta E = -11.28$ kcal/mol) compared to the other three dimers studied (Figures 5b-d). Indeed, as illustrated experimentally by Patrick and Prosser,[26] benzene and hexafluorobenzene are known to form energetically favorable dimeric units due to opposite electric quadrupole moments (benzene, $Qzz = -29.0 \times 10^{-40}$ C m^2 and hexafluorobenzene, $Qzz = 31.7 \times 10^{-40}$ C m^2)[61] which provides support for these observed interactions in **2**. Additionally, similar to that observed in the solid state of **2**, arene-perfluoroarene-based dimers are typically arranged in slightly shifted (π-stacked) sandwichlike structures with alternating molecular positive and negative quadrupole moments.[63] Referring to the experimentally determined lateral configuration of **2** (Figure 2e), it is clear that every pair of molecules belonging to the same layer is precisely arranged to maximize these face-to-face interactions between unsubstituted and tetrafluorosubstituted units, presumably induced by the large stabilization energy of −11.28 kcal/mol calculated for this configuration. Thus, these energetically dominant interactions effectively drive the self-assembly of the system.

While the lateral interactions can be explained on the basis of face-to-face arene-perfluoroarene interactions, the radial geometry of the macrocycles prohibits these interactions in the vertical direction. Bearing this in mind, we next sought to understand the origin as well as identity of the secondary interactions that drive the vertical assembly. Accordingly, a vertical nanohoops dimer was identified, and the interaction energy was, to our surprise, determined to be higher (23.08 vs 11.28 kcal/mol) than that determined for the lateral dimeric structure. As discussed in the solid-state analysis, we attribute this result to multiple C−H—F interactions. The aryl C−H—F contacts here are comprised between 2.53 and 2.85 Å, depending on the relative orientations between interacting rings, and are thus found below or close to the sum of the van der Waals radii of H (120 pm) and F (147 pm). Importantly, this dimer displays a remarkably large interaction energy of −23.08 kcal/mol as compared to the determined value of −17.32 kcal/mol for the corresponding offset-tubular dimer (Figure S16) found in the herringbone-like packing of the

DOI: 10.1021/acs.joc.9b02340
J. Org. Chem. 2020, 85, 129−141

parent hydrocarbon [10]CPP.[56] Intrigued by the unexpectedly large contribution of these C−H−F interactions, we then examined the theoretical energetic repercussions of systematically removing tetrafluorinated aryl rings from the vertical dimer of **2**. As expected, a consistent decrease in interaction energy was observed in going from four to zero tetrafluorinated aryl rings (Figure 6b-e). To examine this result experimentally,

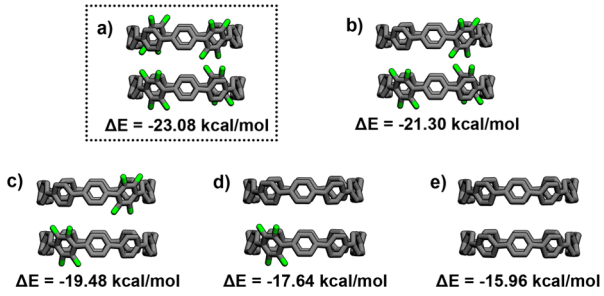

Figure 6. a) Calculated interaction energy for the vertical dimer extracted from the crystal structure of nanohoop **2**, along with the structures and respective interaction energies for this dimer upon the removal of fluorine atoms.

we then prepared a [10]CPP derivative embedded with a single tetrafluoro aryl ring (Scheme S2). As revealed by single crystal X-ray analysis, nanohoop **S2** packed into a herringbone type motif (Figure S6), confirming our theoretical predictions, and, perhaps more importantly, suggesting that this approach may act as a predictive design tool for future investigations. Particularly noteworthy is the modest difference in interaction energy (<2 kcal/mol) between the tubular dimer shown in Figure 6e (i.e., a theoretical solid-state columnar arrangement of [10]CPP) and that determined for the offset-tubular arrangement of [10]CPP (Figure S16). This modest difference provides a rationale for the observed solid-state arrangement of [10]CPP, where polymorphism can be predicted. Ultimately, these findings highlight important considerations when designing these cylindrical structures. Additionally, while this analysis was carried out with **2**, we found that the vertical, secondary interactions in **1** (Figure S17) also had stronger interaction energies than those in the lateral direction (Figure S18)—a feature that likely plays a role in the observed packing of C_{60}@**2**, where face-to-face interactions are not present.

CONCLUSION AND OUTLOOK

In conclusion, we have presented a scalable, size-selective strategy for accessing functional CNT mimic systems. Two novel fluorinated nanohoops (**2** and **3**) were synthesized via a general route using common intermediates, and a new synthetic approach was developed to access previously reported nanohoop **1** on the gram scale. Through X-ray crystallographic analysis, it was determined that nanohoops **1**, **2**, and **3** all self-assemble into CNT mimic systems in the solid state via organofluorine interactions and boast uniform channel diameters defined by the diameters of their respective constituent nanohoops. Aside from the aesthetic similarities between CNTs and the mimic systems disclosed herein, CNT-like properties were also found to emerge as a result of tubular nanohoop alignment. Specifically, nanohoop **2** was shown capable of linear C_{60} alignment, while nanohoop **1** exhibits accessible channels at 77 K with a BET surface area of 608 $m^2 g^{-1}$. Neither of these functionalities are observed in the analogous nonfluorinated nanohoop systems, implying that the arene-perfluoroarene and C−H—F interactions observed in the crystal structures of the CNT mimics are effective in maintaining a tubular architecture. We further supported this hypothesis via a theoretical analysis of the crystal structure of nanohoop **2**, the results of which strongly suggest that organofluorine interactions are indeed energetically dominant in the self-assembly of the fluorinated nanohoop systems. The ability to fabricate these CNT mimics in a discrete, size-selective fashion is expected to benefit studies in nanofluidics and general nanoscale confinement, where access to atomically precise nanopores is difficult due to the inability to selectively produce CNTs or graphene nanopores. Furthermore, we believe the combined experimental and theoretical analysis of the CNT mimics presented may serve as an initial blueprint for the predictable design of other tubular systems based on the self-assembly of curved macrocycles, opening the door to a variety of new precision nanomaterials.

EXPERIMENTAL SECTION

General Information. ^{1}H NMR spectra were recorded at 500 MHz on a Varian VNMR spectrometer, 500 MHz on a Bruker spectrometer, or 600 MHz on a Bruker spectrometer. All ^{1}H NMR spectra are referenced to TMS (δ 0.00 ppm), CH_2Cl_2 (δ 5.32 ppm), or $(CH_3)_3CO$ (δ 2.05 ppm). All ^{13}C NMR spectra are references to a residual $CHCl_3$ (δ 77.16 ppm), CH_2Cl_2 (54.00 ppm), or $(CH_3)_3CO$ (δ 29.84 ppm). All ^{19}F spectra were indirectly referenced via the Bruker TopSpin 3.5 software suite to $CFCl_3$. All reagents were obtained commercially and used without further purification unless otherwise noted. All glassware was flame-dried and cooled under an inert atmosphere of nitrogen unless otherwise noted. Moisture sensitive reactions were carried out under an inert atmosphere of nitrogen using standard syringe/septa technique. Absorbance spectra for **2** and **3** were collected in dichloromethane (DCM) in a 1 cm quartz cuvette on an Agilent Cary 60 UV−vis spectrophotometer. The emission spectra for **2** and **3** were collected in DCM on a Horiba Jobin Yvon Fluoromax-4 fluorometer. Silica column chromatography was conducted with Zeochem Zeoprep 60 Eco 40-63 μM silica gel while alumina chromatography utilized Sorbent Technologies 50-200 um Basic Activity II−II alumina. Intermediates **4a**, **4b**, **5**, and **8** were prepared as reported in ref 25. Intermediates **5S** and **10** were prepared as reported in ref 64.

Specific experimental details for the computational studies included in both the manuscript and Supporting Information can be found in ref 56.

Synthetic Procedures. *Synthesis of Macrocycle **6a**.* To a flame-dried 250 mL round-bottom flask equipped with a stir bar was added **4a** (0.268 g, 2.36 mmol, 1.00 equiv), **5** (0.290 g, 2.36 mmol, 1.00 equiv), and SPhos-Pd-G2 (16.9 mg, 0.0236 mmol, 0.100 equiv). The flask was evacuated and backfilled with N_2 5 times, followed by addition of 1,4-dioxane (118 mL). This solution was then vigorously sparged with N_2 for 2 h at which point the solution was placed into an oil bath at 80 °C. At this point, an aqueous solution of 2 M K_3PO_4 (11.8 mL, 23.6 mmol, 10.0 equiv) was added, quickly turning the colorless solution bright yellow. The solution was allowed to stir for 1 h, at which point the solution was allowed to cool to room temperature followed by removal of the solvent via rotary evaporation. The resulting yellow/brown oil was extracted with hexanes (3 × 100 mL), followed by washing of the combined organic phases with H_2O (3 × 100 mL), brine (1 × 100 mL), and finally placed over sodium sulfate. After solvent removal, the brown oil was dissolved in hexanes and then filtered over a fritted funnel. The brown solids were washed with plenty of hexanes, and the resulting yellow filtrate was concentrated to a yellow oil. The addition of acetone caused the precipitation of a white solid, which after collection via filtration and washing with acetone yielded **6a** as a white solid (0.207 g, 45%). ^{1}H NMR (500 MHz, $CDCl_3$) δ 7.15 (d, J = 8.4 Hz, 8H), 7.07 (d, J = 8.5

DOI: 10.1021/acs.joc.9b02340
J. Org. Chem. 2020, 85, 129−141

Hz, 8H), 6.37 (d, J = 10.2 Hz, 8H), 6.00 (d, J = 10.4 Hz, 8H), 1.01−0.81 (m, 72H), 0.76−0.53 (m, 48H). $^{13}C\{^1H\}$ NMR (126 MHz, $CDCl_3$) δ 144.1, 139.7, 133.5, 129.0, 127.0, 125.5, 71.3, 70.2, 7.2, 6.9, 6.6, 6.3. ^{19}F NMR (471 MHz, $CDCl_3$) δ −136.43 (s). δ LRMS (TOF, MALDI) (m/z): $[M]^+$ calculated for $C_{108}H_{152}O_8F_8Si_8$, 1952.951; found, 1954.126.

Synthesis of Nanohoop ***2***. To a flame-dried 50 mL round-bottom flask equipped with a stir bar was added **6a** (0.077 g, 0.0365 mmol, 1.00 equiv) followed by THF (20 mL). To this solution was then added glacial acetic acid (0.105 mL, 1.83 mmol, 50.0 equiv), followed by tetrabutylammonium fluoride (1 M in THF, 0.914 mL, 0.914 mmol, 25 equiv) dropwise. The resulting colorless solution was then stirred for 18 h at which point H_2O (10 mL) was added, followed by removal of THF via rotary evaporation. The white solid was then filtered and washed with H_2O (30 mL) to afford the deprotected intermediate as a white solid. Without further purification, the intermediate was placed in a flame-dried 50 mL round-bottom flask equipped with a stir bar followed by THF (8 mL). To the resulting cloudy-white solution was added 1,8-diazabicyclo[5.4.0]undec-7-ene (0.027 mL, 0.292 mmol, 8 equiv), followed by PBr_3 (0.044 mL, 0.292 mmol, 8 equiv), resulting in an obvious white precipitate. After ∼5 min of stirring, anhydrous $SnCl_2$ (0.055 g, 0.292 mmol, 8 equiv) was added as a solid, turning the solution yellow. After 1 h of stirring, the solution was quenched with 10% NaOH (5 mL), and THF was removed via rotary evaporation. To the resulting yellow suspension was added 125 mL of H_2O, followed by excessive extractions with DCM (6 × 50 mL). This was followed by washes with H_2O (3 × 50 mL) and brine (1 × 50 mL). The organic layer was then dried over sodium sulfate and filtered, followed by solvent removal via rotary evaporation. Purification via column chromatography (0−40% DCM/Hexanes), using basic alumina as the stationary phase, afforded **2** as an off-white solid (0.019 g, 58%). ^1H NMR (500 MHz, $CDCl_3$) δ 7.71−7.45 (m, 32H). ^{19}F NMR (471 MHz, $CDCl_3$) δ −143.52 (s). Due to insolubility, ^{13}C NMR data could not be obtained. δ HRMS (TOF, ES+) (m/z): $[M]^+$ calculated for $C_{60}H_{32}F_8$, 904.2376; found, 904.2380.

Synthesis of Macrocycle ***6b***. To a flame-dried 250 mL round-bottom flask equipped with a stir bar was added **5** (0.334 g, 0.271 mmol, 1.00 equiv), **4b** (0.325 g, 0.271 mmol, 1.00 equiv), and SPhos-Pd-G2 (0.039 g, 0.0542 mmol, 0.200 equiv). The flask was evacuated and backfilled with N_2 5 times, followed by addition of 1,4-dioxane (90 mL). This solution was then vigorously sparged with N_2 for 1 h at which point the solution was placed into an oil bath at 80 °C. At this point, an aqueous solution of 2 M K_3PO_4 (9.03 mL, 4.52 mmol, 17.0 equiv) was added. The solution was allowed to stir for 12 h, after which the solution was brought to room temperature, and the solvent was removed under reduced pressure. Water (50 mL) was added, followed by extraction with DCM (3 × 50 mL). The combined organic phases were washed with water (3 × 50 mL) and brine (1 × 50 mL) and dried over sodium sulfate. The solvent was removed via rotary evaporation, and the resulting brown solid was purified via column chromatography (0−40% DCM/Hexanes) using basic alumina as the stationary phase. This afforded **6b** as a white solid (0.199 g, 35%). ^1H NMR (500 MHz, $CDCl_3$) δ 7.36 (d, J = 7.9 Hz, 8H), 7.28 (d, J = 7.7 Hz, 8H), 6.40 (d, J = 9.7 Hz, 8H), 5.99 (d, J = 9.3 Hz, 8H), 0.99 (t, J = 7.8 Hz, 36H), 0.94 (t, J = 8.0 Hz, 36H), 0.69 (q, J = 7.9 Hz, 24H), 0.61 (q, J = 7.8 Hz, 24H). $^{13}C\{^1H\}$ NMR (126 MHz, $CDCl_3$) δ 144.1, 139.6, 139.1, 133.2, 128.6, 127.1, 126.6, 125.7, 71.4, 69.9, 7.1, 6.8, 6.4, 6.2. ^{19}F NMR (471 MHz, $CDCl_3$) δ −136.37 (s). δ HRMS (MALDI, TOF), m/z calculated for $C_{120}H_{160}F_8O_8Si_8$ $(M)^+$ 2106.02, found 2106.02.

Synthesis of Nanohoop ***3***. To a flame-dried 100 mL round-bottom flask equipped with a stir bar was added **6b** (0.036 g, 0.0171 mmol, 1.00 equiv) followed by THF (10 mL). To this solution was then added glacial acetic acid (0.049 mL, 0.854 mmol, 50.0 equiv), followed by tetrabutylammonium fluoride (1 M in THF, 0.427 mL, 0. mmol, 25 equiv) dropwise. The resulting colorless solution was then stirred for 18 h at which point H_2O (10 mL) was added, followed by removal of THF via rotary evaporation. The white solid was then filtered and washed with H_2O (30 mL) to afford the deprotected intermediate as a white solid. Without further purification, the intermediate was placed in a flame-dried 50 mL round-bottom flask equipped with a stir bar followed by THF (8 mL). To the resulting cloudy-white solution was added 1,8-diazabicyclo[5.4.0]undec-7-ene (0.020 mL, 0.137 mmol, 8 equiv), followed by PBr_3 (0.013 mL, 0.137 mmol, 8 equiv) dropwise, resulting in a white precipitate. After ∼5 min of stirring, anhydrous $SnCl_2$ (0.026 g, 0.137 mmol, 8 equiv) was added as a solid, turning the solution yellow. After 1 h of stirring, the solution was quenched with 10% NaOH (5 mL), and THF was removed via rotary evaporation. To the resulting yellow suspension was added 125 mL of H_2O, followed by excessive extractions with DCM (6 × 50 mL). This was followed by washes with H_2O (3 × 50 mL) and brine (1 × 50 mL). The organic layer was then dried over sodium sulfate and filtered, followed by solvent removal via rotary evaporation. Purification via column chromatography (0−40% DCM/Hexanes) afforded **3** as an off-white solid (0.005 g, 28%). ^1H NMR (500 MHz, $CDCl_3$) δ 7.70−7.63 (m, 30H), 7.57 (d, J = 8.4 Hz, 10H). ^{19}F NMR (471 MHz, $CDCl_3$) δ −143.86 (s). Due to insolubility, ^{13}C NMR data could not be obtained. δ HRMS (MALDI, TOF), m/z calculated for $C_{72}H_{40}F_8$ $(M)^+$ 1056.30, found 1056.30.

Synthesis of ***7S***. (See Scheme S1.) To a 250 mL flame-dried flask was added **10** (18.56 g, 28.0 mmol, 2 equiv), 1,4-dibromo-2,3,5,6-tetrafluorobenzene (4.27 g, 14.0 mmol, 1 equiv), and [1,1′-bis(diphenylphosphino)ferrocenedichloropalladium (1.01 g, 1.39 mmol, 0.100 equiv). After the solids were added, the flask was evacuated and backfilled with nitrogen 3 times. The flask was then purged with N_2 for 20 min. 1,4-Dioxane (100.0 mL) was then added to the flask, after which aqueous 2 M K_3PO_4 (0.660 mL, 1.32 mmol, 5.5 equiv), sparged for 1 h prior to use, was added. The solution was then placed in an 80 °C oil bath and allowed to stir for 12 h. The next day, the reddish-black solution was allowed to come to room temperature before removing the solvent under reduced pressure. The resulting reddish-black sludge was dissolved in DCM and run through a plug of Celite with a small pad of silica on top. This was followed by removal of DCM solvent from the eluent via rotary evaporation. The resulting yellow oil was washed with MeOH, causing the product to precipitate as a white solid. Vacuum filtration, followed by additional MeOH rinses, afforded **7S** as a white solid (14.70 g, 88%). ^1H NMR (500 MHz, $CDCl_3$) δ 7.45 (dd, 8H), 7.32 (d, J = 8.5 Hz, 4H), 7.26 (d, 4H), 6.09−5.97 (dd, 8H), 0.97 (dt, J = 11.2, 7.9 Hz, 36H), 0.65 (dq, J = 21.6, 7.9 Hz, 24H). $^{13}C\{^1H\}$ NMR (126 MHz, $CDCl_3$) δ 146.8, 144.5, 133.1, 131.6, 131.5, 130.0, 128.3, 127.4, 126.4, 126.3, 71.4, 71.1, 7.0, 6.5. ^{19}F NMR (471 MHz, $CDCl_3$) δ −144.35. MS could not be obtained.

Synthesis of ***7***. To a 100 mL flame-dried flask was added $Pd(OAc)_2$ (0.135 g, 0.602 mmol, 0.05 equiv), 2-dicyclohexylphosphino-2′6′-dimethoxybiphenyl (0.618 g, 1.50 mmol, 0.125 equiv), bis(pinacolato)diboron (15.30 g, 60.2 mmol, 5 equiv), **7S** (14.45 g, 12.0 mmol, 1 equiv), and K_3PO_4 (5.91 g, 60.2 mmol, 5 equiv). After the solids were added, the flask was evacuated and backfilled with nitrogen 5 times. The flask was then purged with N_2 for 20 min. 1,4-Dioxane (100.0 mL) was then added to the flask, and the solution was sparged for 20 min before being placed in an 80 °C oil bath overnight. The next day, the black solution was brought to room temperature, and the solvent was removed under reduced pressure. The resulting black sludge was dissolved in DCM and run through a plug of Celite with a small pad of silica on top. After removing the DCM solvent from the eluent via rotary evaporation, the resulting dark-orange oil was washed with methanol, causing the product to precipitate as a white solid. Vacuum filtration afforded **7** as a white solid (15.54 g, 93%). ^1H NMR (500 MHz, $CDCl_3$) δ 7.74 (d, J = 8.0 Hz, 4H), 7.45 (d, J = 8.4 Hz, 4H), 7.40 (d, J = 8.2 Hz, 8H), 6.05 (d, J = 10.1 Hz, 4H), 5.99 (d, J = 10.1 Hz, 4H), 1.33 (s, 24H), 0.94 (dt, J = 25.1, 7.9 Hz, 36H), 0.67 (q, J = 7.9 Hz, 12H), 0.57 (q, J = 7.9 Hz, 12H). $^{13}C\{^1H\}$ NMR (126 MHz, $CDCl_3$) δ 149.0, 147.0, 145.0, 143.2, 134.8, 131.6, 131.4, 129.9, 128.2, 126.3, 126.0, 125.9, 125.3, 83.8, 71.5, 24.9, 7.1, 7.0, 6.5, 6.4. ^{19}F NMR (471 MHz, $CDCl_3$) δ −144.37. δ HRMS (TOF, ES+) (m/z): $[M]^+$ calculated for $C_{78}H_{108}B_2O_8F_4NaSi_4$, 1405.7141; found, 1405.7163.

DOI: 10.1021/acs.joc.9b02340
J. Org. Chem. 2020, 85, 129−141

Synthesis of ***9***. To a flame-dried 2000 mL round-bottom flask equipped with a stir bar was added **7** (14.44 g, 10.40 mmol, 1.00 equiv), **8** (10.80 g, 10.40 mmol, 1.00 equiv), and SPhos-Pd-G2 (1.50 g, 2.08 mmol, 0.200 equiv). The flask was evacuated and backfilled with N_2 5 times, followed by 30 min of purging with N_2. Next, 1,4-dioxane (1000 mL) was added to the flask via cannula to afford a 10 mM solution. This solution was then vigorously sparged with N_2 for 2 h at which point the solution was placed into an oil bath at 80 °C. At this point, an aqueous solution of 2 M K_3PO_4 (103.9 mL, 207.8 mmol, 20.0 equiv) was added. The solution was allowed to stir for 12 h, after which the solution was brought to room temperature, and the solvent was removed under reduced pressure. The resulting brown oil was dissolved in DCM and run through a plug of Celite with a small pad of silica on top. The eluent was then dried via rotary evaporation to afford a sticky white solid. Purification via column chromatography (0−40% DCM/Hexanes) afforded **9** as a white solid (4.46 g, 22%) (alternatively, the crude material can be washed with hexanes to precipitate the product at a loss of yield). ^{1}H NMR (500 MHz, $CDCl_3$) δ 7.53 (d, J = 8.2 Hz, 12H), 7.45 (d, J = 8.0 Hz, 12H), 6.10 (s, 12H), 0.99 (t, J = 7.9 Hz, 54H), 0.68 (q, J = 7.9 Hz, 36H). ^{13}C{^{1}H} NMR (126 MHz, $CDCl_3$) δ 147.0, 145.2, 143.1, 131.5, 130.0, 126.4, 126.1, 71.5, 7.1, 6.5. ^{19}F NMR (471 MHz, $CDCl_3$) δ −144.38. MALDI TOF, m/z calculated for $C_{108}H_{126}F_{12}O_6Si_6$ $(M)^+$ 1915.80, found 1915.96.

Synthesis of ***1***. To a flame-dried 50 mL round-bottom flask equipped with a stir bar was added **9** (0.174 g, 0.091 mmol, 1.00 equiv) followed by THF (10 mL). To this solution was then added tetrabutylammonium fluoride (1 M in THF, 2.27 mL, 2.27 mmol, 25.0 equiv) dropwise. This solution was then stirred for 2 h at which point H_2O (10 mL) was added, followed by removal of THF via rotary evaporation. The resulting suspension was vacuum filtered, washed with water, and allowed to fully dry. Without further purification, the crude white solid was placed in a flame-dried 250 mL round-bottom flask equipped with a stir bar followed by THF (100 mL). The flask was then placed in an ice bath (0 °C) and allowed to cool for 30 min. After 30 min, 1,8-diazabicyclo[5.4.0]undec-7-ene (0.027 mL, 0.292 mmol, 8 equiv) was added, followed by PBr_3 (0.044 mL, 0.292 mmol, 8 equiv) dropwise, resulting in a white precipitate. After ∼5 min of stirring, anhydrous $SnCl_2$ (0.055 g, 0.292 mmol, 8 equiv) was added as a solid, turning the solution yellow. After 1 h of stirring, a majority of the THF solvent was removed via rotary evaporation, and the concentrated reaction mixture was poured directly onto a basic alumina plug. Flushing the plug with DCM caused only the product to elute. The eluent was dried under reduced pressure to afford **1** as an off-white solid (1.06 g, 40%). ^{1}H NMR (500 MHz, $CDCl_3$) δ 7.69 (d, J = 6.2 Hz, 24H), 7.59 (d, J = 8.2 Hz, 12H). ^{19}F NMR (471 MHz, $CDCl_3$) δ −143.82 (s). Due to insolubility, ^{13}C NMR data could not be obtained. MALDI TOF, m/z calculated for $C_{72}H_{36}F_{12}$ $(M)^+$ 1128.2625, found 1128.0620.

Synthesis of ***6S***. (See Scheme S2.) To a flame-dried 250 mL round-bottom flask equipped with a stir bar was added **4a** (0.338 g, 2.92 mmol, 1.00 equiv), **5S** (0.330 g, 2.92 mmol, 1.00 equiv), and SPhos-Pd-G2 (20.0 mg, 0.0292 mmol, 0.100 equiv). The flask was evacuated and backfilled with N_2 5 times, followed by addition of 1,4-dioxane (146 mL). This solution was then vigorously sparged with N_2 for 2 h at which point the solution was placed into an oil bath at 80 °C. At this point, an aqueous solution of 2 M K_3PO_4 (14.6 mL, 29.2 mmol, 10.0 equiv) was added, quickly turning the colorless solution bright yellow, turning to a white suspension over the course of 1 h. The solution was allowed to stir for 2 h, at which point the solution was cooled to room temperature followed by removal of the solvent via rotary evaporation. The resulting yellow/brown oil aqueous phase was extracted with hexanes (3 × 100 mL), followed by washing of the combined organic phases with H_2O (3 × 100 mL), brine (1 × 100 mL), and finally placed over sodium sulfate. After solvent removal, the brown oil was dissolved in hexanes and then filtered using a fritted funnel. The brown solids were washed with plenty of hexanes, and the resulting yellow filtrate was concentrated to a yellow oil. The yellow oil was loaded onto silica gel (0−40% DCM/Hexanes) to afford macrocycle **6S** as a white solid (0.203 g, 37%). ^{1}H NMR (600 MHz, $CDCl_3$) δ 7.33 (d, J = 8.4 Hz, 4H), 7.29 (d, J = 8.4 Hz, 4H), 7.26−7.20 (m, 8H), 7.12 (s, 4H), 6.40 (d, J = 10.1 Hz, 4H), 6.00 (d, J = 10.3 Hz, 4H), 5.95 (d, J = 10.3 Hz, 4H), 5.92 (d, J = 10.2 Hz, 4H), 0.99−0.87 (m, 72H), 0.62 (m, 48H). ^{13}C{^{1}H} NMR (151 MHz, $CDCl_3$) δ 146.2, 145.0, 144.9, 144.3, 139.7, 139.6, 133.4, 131.8, 131.6, 131.5, 131.3, 128.8, 128.2, 127.0, 126.8, 126.3, 125.9, 125.9, 125.7, 125.7, 123.9, 71.6, 71.4, 71.6, 70.1, 7.2, 7.2, 6.9, 6.6, 6.6, 6.3. ^{19}F NMR (471 MHz, $CDCl_3$) δ −136.43 (s). δ LRMS (TOF, MALDI) (m/z): $[M]^+$ calculated for $C_{108}H_{156}O_8F_4Si_8$, 1880.99; found, 1882.1.

Synthesis of ***2S***. (See Scheme S2.) To a flame-dried 100 mL round-bottom flask equipped with a stir bar was added **6S** (0.203 g, 0.108 mmol, 1.00 equiv) followed by THF (20 mL). To this solution was then added glacial acetic acid (0.620 mL, 10.8 mmol, 100.0 equiv), followed by tetrabutylammonium fluoride (1 M in THF, 2.16 mL, 2.16 mmol, 20.0 equiv) dropwise. The resulting colorless solution was then stirred for 18 h at which point H_2O (10 mL) was added, followed by removal of THF via rotary evaporation. The white solid was then filtered and washed with H_2O (30 mL) and DCM (3 × 10 mL) to give crude, deprotected **6S** (0.0941 g, 90%). The resulting white solid then added to a flame-dried 100 mL round-bottom flask equipped with a stir bar, followed by THF (40 mL). To this suspension was added H_2SnCl_4 (0.40 M in THF, 0.0971 mmol, 1.21 mL, 5.00 equiv), resulting in a faint-yellow/white suspension which was stirred at room temperature for 18 h. Aqueous (18 w/w%) ammonia (10 mL) was added followed by filtration using a fritted funnel. The resulting faint blue filtrate was then collected in a round-bottom flask, followed by removal of THF via rotary evaporation and gave an off-white/teal solid. This solid was then dissolved in DCM (100 mL), washed with H_2O (3 × 50 mL) and brine (1 × 50 mL), and then placed over sodium sulfate. After removal of solvent, the resulting solid was loaded onto silica gel (0−100% DCM/Hexanes) to give **2S** as an off-white/yellow solid (17.9 mg, 20%). ^{1}H NMR (500 MHz, $CDCl_3$) δ 7.70−7.47 (m, 36H). ^{13}C{^{1}H} NMR (126 MHz, $CDCl_3$) δ 140.9, 138.6, 138.4, 138.3, 138.2, 138.2, 138.0, 137.9, 130.9, 127.8, 127.5, 127.4, 127.4, 127.3, 127.0, 126.8. ^{19}F NMR (471 MHz, $CDCl_3$) δ −143.54 (s). δ HRMS (TOF, ES+) (m/z): [M]+ calculated for $C_{60}H_{36}F_4$, 832.2753; found, 832.2748.

Binding Constant (K_a) Determination. Binding constants were determined via fluorescence quenching experiments as reported by the Sessler[65] and Yamago[38] groups. In a typical experiment, a solution of C_{60} in toluene (1.01×10^{-5} mol L^{-1}) was added to a solution of fluorinated nanohoop **1** in toluene (5.00×10^{-7} mol L^{-1}). The change in fluorescence emission intensity at 460 nm was then monitored for each addition (Figure S3).

The K_a was then determined by fitting the data to eq 1

$$F/F_o = \left(1 + \frac{k_f}{k_{sf}} * K_a * [C_{60}]\right)/(1 + K_a * [C_{60}]) \quad (1)$$

where F, F_o, k_f, k_s, K_a, and $[C_{60}]$ denote fluorescence intensity, fluorescence of fluorinated nanohoop **1** prior to the addition of C_{60}, a proportionality constant of the complex, a proportionality constant of the host, the binding constant of C_{60}, and the concentration of C_{60}, respectively. The data from Figure S3 have been fit to eq 1 and are shown in Figure S4.

Crystallographic Data. Diffraction intensities for **2** were collected at 173 K on a Bruker Apex2 CCD diffractometer using an *Incoatec* Cu *IμS* source, CuKα radiation, 1.54178 Å. Space groups were determined based on systematic absences. Absorption corrections were applied by SADABS.[66] Structures were solved by direct methods and Fourier techniques and refined on $F2$ using full matrix least-squares procedures. All non-H atoms were refined with anisotropic thermal parameters except for the C and O atoms in solvent THF molecules in **2** which were refined with isotropic thermal parameters. All H atoms in **2** were refined in calculated positions in a rigid group model. Six THF molecules are in **2**, with two THF molecules being located outside the hoop. Four THF molecules in **2** are located inside the hoops. Positions of the THF molecules in **2** in the hoop were found on the residual density map and refined. Thermal atomic parameters for THF molecules located in the hoop in

DOI: 10.1021/acs.joc.9b02340
J. Org. Chem. 2020, 85, 129−141

2 are large and show that these molecules seem to be disordered. One short H···H contact between these THF molecules (H18c···H21C, 1.94 Å) also indicates that the THF molecules located in the hoop are disordered. X-ray diffraction from crystals of **2** at high angles was very weak. Even by using a strong *Incoatec* Cu *IμS* source it was possible to collect diffraction data only up to $2\theta_{max}$ = 98.79°. Regardless, the collected data provide an appropriate number of measured reflections per refined parameters: 7163 reflections per 833 refined parameters. All calculations were performed by the Bruker SHELXL-2014/7 package.[67]

Diffraction intensities for **3** were collected at 173 K on a Bruker Apex2 CCD diffractometer using CuKα radiation, λ = 1.54178 Å. Space groups were determined based on intensity statistics. Absorption corrections were applied by SADABS.[66] Structures were solved by direct methods and Fourier techniques and refined on F^2 using full matrix least-squares procedures. All non-H atoms were refined with anisotropic thermal parameters. All H atoms were refined in calculated positions in a rigid group model. There are two symmetrically independent main molecules in the crystal structure. The molecules form columns in the crystal. Two solvent molecules CH_2Cl_2 filling a space between the columns in the packing are ordered. These solvent molecules were found and refined. Three pentane and two dichloromethane solvent molecules filling a space inside the hoop are highly disordered and were treated by SQUEEZE.[68] Correction of the X-ray data by SQUEEZE is 490 electron/cell; the required value is 420 electron/cell for four CH_2Cl_2 and six C_5H_{12} molecules in the full unit cell. All calculations were performed by the Bruker SHELXL-2014 package.[67]

Diffraction intensities for **2**@C_{60} were collected at 173 K on a Bruker Apex2 CCD diffractometer using an *Incoatec* Cu *IμS* source, CuKα radiation, 1.54178 Å. Space groups were determined based on systematic absences. Absorption corrections were applied by SADABS.[66] Structures were solved by direct methods and Fourier techniques and refined on *F*2 using full matrix least-squares procedures. All non-H atoms were refined without any restrictions and with anisotropic thermal parameters. H atoms in the hoop were refined in calculated positions in a rigid group model. The crystal structure has additional solvent molecules which are highly disordered and fill out a space between the main molecules. Based on the residual density map we suggest that in the crystal structure there are highly disordered solvent molecules; one toluene molecule is disordered in a general position, and four O_2Et_2 solvent molecules are disordered over an inversion center. These disordered solvent molecules have been treated by SQUEEZE,[68] but they are added to the formula of the compound. Correction of the X-ray data by SQUEEZE is 1224 electron/unit cell; the required number of electrons is 1072 for eight toluene and 16 diethyl ether molecules in the full unit cell. Comments about using SQUEEZE have been added in the final CIF file. All calculations were performed by the Bruker SHELXL-2014/7.[67]

Diffraction intensities for **2S** were collected at 173 K on a Bruker Apex2 CCD diffractometer using CuKα radiations, 1.54178 Å. Space groups were determined based on systematic absences. The beta angle in the monoclinic system is close to 90°, but the structure was determined in the lowest possible space group *P*21/*c* to avoid a possible disorder due to using high symmetry. Absorption corrections were applied by SADABS.[66] Structures were solved by direct methods and Fourier techniques and refined on *F*2 using full matrix least-squares procedures. All non-H atoms were refined with anisotropic thermal parameters. All H atoms were refined in calculated positions in a rigid group model. Refinement of the structure without restrictions shows that in all C_6-rings of the hoop the C−H distances are longer vs the standard C−H distance of 0.95 Å and C−F bond lengths are shorter vs the standard C−F distance of 1.35 Å. It indicates that four F atoms in the structure are disordered over many positions. After checking several options for the disorder, we found that the model in which four F atoms are disordered over all ten C6-rings does not provide the best final data. Thus, the final refinement has been done for the model where four F atoms are disordered over six positions corresponding to the six C_6-rings which are slightly out from the central part of the hoop. Such a S32 conformation seems to be related to more steric repulsions for C_6F_4 groups vs the C_6H_6 groups. The disordered H and F atoms were taken in the refinement with appropriate occupation factors. The structure was refined with restrictions; the standard C−H and C−F distances were used as the targets for corresponding bonds and C_6F_4 groups were refined as flat groups. RIGU restriction has been also applied for thermal parameters. The residual density map shows that inside the main hoop there are one or two disordered solvent molecules. Our attempts to model this disorder with full or partially occupied positions of pentane/hexane molecules failed. These disordered solvent molecules have been treated by SQUEEZE.[68] The correction of the X-ray data by SQUEEZE, 80 electrons, corresponds to two possible solvent pentane molecules, C_5H_{12}, 84 electrons. Taking into account that these positions could be partially occupied, only one pentane molecule per the main molecule was added into the final formula. Diffraction from crystals of **2S** was very weak at high angles. Even using a strong *Incoatec IμS* Cu-source it was possible to collect diffraction data only to $2\theta_{max}$ = 99.64°. Regardless, the collected data provide in the refinements an appropriate number of reflections per independent refined parameters. All calculations were performed by the Bruker SHELXL-2014 package.[67]

Crystallographic Data for **2**. $C_{84}H_{80}F_8O_6$, $C_{60}H_{32}F_8{\cdot}6(OC_4H_8)$, M = 1337.48, 0.12 × 0.08 × 0.05 mm, T = 173(2) K, monoclinic, space group *P*21/*c*, a = 13.4645(7) Å, b = 19.5258(12) Å, c = 26.8045(16) Å, β = 94.711(4)°, V = 7023.2(7) Å^3, Z = 4, D_c = 1.265 Mg/m^3, μ(Cu) = 0.764 mm^{-1}, F(000) = 2816, $2\theta_{max}$ = 98.79°, 26273 reflections, 7163 independent reflections [R_{int} = 0.0655], R1 = 0.0769, wR2 = 0.2115, and GOF = 1.021 for 7163 reflections (833 parameters) with $I > 2\sigma(I)$, R1 = 0.1071, wR2 = 0.2453, and GOF = 1.022 for all reflections, max/min residual electron density +0.559/−0.506 eÅ^{-3}.

Crystallographic Data for **3**. $C_{91}H_{84}Cl_8F_8$, $C_{72}H_{40}F_8{\cdot}4(CH_2Cl_2){\cdot}3(C_5H_{12})$, M = 1613.18, 0.15 × 0.08 × 0.03 mm, T = 173(2) K, triclinic, space group *P*-1, a = 13.3910(4) Å, b = 20.0066(6) Å, c = 20.2292(6) Å, α = 119.204(2)°, β = 97.369(2)°, γ = 102.306(6)°, V = 4447.3(2) Å^3, Z = 2, D_c = 1.205 Mg/m^3, μ(Cu) = 2.795 mm^{-1}, F(000) = 1676, $2\theta_{max}$ = 133.39°, 61640 reflections, 15617 independent reflections [R_{int} = 0.0524], R1 = 0.0499, wR2 = 0.1240, and GOF = 1.045 for 15617 reflections (775 parameters) with $I > 2\sigma(I)$, R1 = 0.0691, wR2 = 0.1313, and GOF = 1.045 for all reflections, max/min residual electron density +0.434/−0.404 eÅ^{-3}.

Crystallographic Data for **2**@C_{60}. $C_{150}H_{88}F_8O_4$, $C_{120}H_{32}F_8{\cdot}4(OC_4H_{10}){\cdot}2(C_7H_8)$, M = 2106.20, 0.12 × 0.06 × 0.02 mm, T = 173(2) K, monoclinic, space group *C*2/*c*, a = 25.1372(10) Å, b = 20.9252(9) Å, c = 19.7816(8) Å, β = 108.436(2)°, V = 9871.1(7) Å^3, Z = 4, D_c = 1.417 Mg/m^3, μ(Cu) = 0.759 mm^{-1}, F(000) = 4368, $2\theta_{max}$ = 133.13°, 39936 reflections, 8726 independent reflections [R_{int} = 0.0514], R1 = 0.0964, wR2 = 0.2870, and GOF = 1.030 for 8726 reflections (577 parameters) with $I > 2\sigma(I)$, R1 = 0.1143, wR2 = 0.3028, and GOF = 1.030 for all reflections, max/min residual electron density +1.271/−0.391 eÅ^{-3}.

Crystallographic Data for **2S**. $C_{65}H_{48}F_4$, M = 905.03, 0.08 × 0.04 × 0.03 mm, T = 173(2) K, monoclinic, space group *P*21/*c*, a = 30.539(2) Å, b = 8.1703(7) Å, c = 21.1171(16) Å, β = 90.018(5)°, V = 5269.0(7) Å^3, Z = 4, D_c = 1.141 Mg/m^3, μ(Cu) = 0.597 mm$_{-1}$, F(000) = 1896, $2\theta_{max}$ = 99.64°, 19529 reflections, 5331 independent reflections [R_{int} = 0.0810], R1 = 0.1338, wR2 = 0.3765, and GOF = 1.194 for 5331 reflections (613 parameters) with $I > 2\sigma(I)$, R1 = 0.2033, wR2 = 0.4214, and GOF = 1.115 for all reflections, max/min residual electron density +0.586/−0.518 eÅ^{-3}.

Thermogravimetric (TGA) Analysis of Nanohoop 1. TGA analysis was carried out on a TA Instruments Thermogravimetric Analyzer (TGA Q500) instrument. A small quantity of nanohoop **1** (4.9870 mg, as measured by the instrument) was placed on an aluminum sample pan, and the sample was heated from room temperature to 600.00 °C at 10.00 °C per minute under N_2 atmosphere (Figure S12).

N_2 Uptake Studies. Gas uptake measurements were performed using a Micromeritics ASAP 2020 Plus. Prior to analysis, samples were evacuated to 2 μtorr and held at 125 °C for approximately 24 h.

DOI: 10.1021/acs.joc.9b02340
J. Org. Chem. 2020, 85, 129−141

Following this activation procedure, sample mass was determined from the difference between the empty sample tube and the sample tube loaded with evacuated material. N_2 uptake was measured isothermally using a liquid nitrogen bath (77 K). Pressure ranges for BET surface area analysis were selected based on guidelines detailed previously.[69] Activation temperatures were chosen based on the high temperatures of thermal stability indicated by thermogravimetric analysis (Figure S12 for nanohoop **1**, ref S4 for [12]CPP). Activation was considered complete when the sample outgassing rate fell below 2 μ torr min^{-1}. See Figures S13 and S14 for N_2 isotherm data and the BET plot, respectively.

Powder X-ray Diffraction (PXRD) Analysis. Powder X-ray Diffraction (PXRD) scans were taken in the range of 1.0−40.0° 2θ on a Bruker D2 Phaser system using a zero-background Si sample holder. PXRD patterns were collected of the as-synthesized powder and of the powder after it was evacuated at 200 °C for 48 h (Figure S15).

Estimation of Cohesive Energies of 2, 2S, and 1. We can estimate the molecular cohesive or lattice energy from the individual interaction energies of the dimers through the following expression

$$U = \Sigma_i^{dimers} m_i \Delta E^{(i)}$$

with m_i being the number of symmetry-unique pairs taking one central molecule as reference, and $\Delta E^{(i)}$ being each of the interaction energies calculated before. The result must be half-divided to avoid a double counting of interactions, and it leads to a value of 65.6 kcal/mol, considerably higher than the value found before for pristine [12]CPP (57.6 kcal/mol).[56]

■ ASSOCIATED CONTENT

Supporting Information

The Supporting Information is available free of charge on the ACS Publications website at DOI: 10.1021/acs.joc.9b02340.

CIF file (CIF)

CIF file (CIF)

CIF file (CIF)

CIF file (CIF)

CIF file (CIF)

Synthetic schemes for intermediate **7** and nanohoop **2S**, synthetic procedures, ^{1}H NMR, ^{13}C NMR, ^{19}F NMR, and mass spectrometry analysis of synthesized compounds, absorption and emission data for **2** and **3** in solution, X-ray crystallography data, experimental details and additional data for C_{60}@**2** quenching experiments and K_a determination, additional N_2 uptake data, and computational data for the solid-state packing of **1** (PDF)

■ AUTHOR INFORMATION

Corresponding Authors

*J.C.S.-G. E-mail: jc.sancho@ua.es.

*R.J. E-mail: rjasti@uoregon.edu.

ORCID

Jeff M. Van Raden: 0000-0002-3505-5170

Erik J. Leonhardt: 0000-0002-5380-2328

A. J. Pérez-Jiménez: 0000-0002-1276-7255

J. C. Sancho-García: 0000-0003-3867-1697

Ramesh Jasti: 0000-0002-8606-6339

Author Contributions

J.M.V.R. and E.J.L. contributed equally.

Notes

The authors declare no competing financial interest.

■ ACKNOWLEDGMENTS

We acknowledge the facilities and staff from the Center for Advanced Materials in Oregon (CAMCOR). The synthesis and structural analysis of **2** and **3** were supported by the National Science Foundation (NSF) under grant numbers CHE-1808791 and CHE-1800586. A.J.P.J. and J.C.S.G. acknowledge the project AICO/2018/175 from the Regional Government (GVA/FSE).

■ REFERENCES

(1) Jariwala, D.; Sangwan, V. K.; Lauhon, L. J.; Marks, T. J.; Hersam, M. C. Carbon Nanomaterials for Electronics, Optoelectronics, Photovoltaics, and Sensing. *Chem. Soc. Rev.* **2013**, *42*, 2824−2860.

(2) Hong, G.; Diao, S.; Antaris, A. L.; Dai, H. Carbon Nanomaterials for Biological Imaging and Nanomedicinal Therapy. *Chem. Rev.* **2015**, *115*, 10816−10906.

(3) Yang, Z.; Ren, J.; Zhang, Z.; Chen, X.; Guan, G.; Qui, L.; Zhang, Y.; Peng, H. Recent Advancement of Nanostructured Carbon for Energy Applications. *Chem. Rev.* **2015**, *115*, 5159−5223.

(4) Holt, J. K.; Park, H. G.; Wang, Y.; Stadermann, M.; Artyukhin, A. B.; Grigoropoulos, C. P.; Noy, A.; Bakajin, O. Fast Mass Transport Through Sub-2-Nanometer Carbon Nanotubes. *Science* **2006**, *312*, 1034−1037.

(5) Tunuguntla, R. H.; Allen, F. I.; Kim, K.; Belliveau, A.; Noy, A. Ultrafast Proton Transport in Sub-1-nm Diameter Carbon Nanotube Porins. *Nat. Nanotechnol.* **2016**, *11*, 639−644.

(6) Radha, B.; Esfandiar, A.; Wang, F. C.; Rooney, A. P.; Gopinadhan, K.; Keerthi, A.; Mischenko, A.; Janardanan, A.; Blake, P.; Fumagalli, L.; Lozada-Hidalgo, M.; Garaj, S.; Haigh, S. J.; Grigorieva, I. V.; Wu, H. A.; Geim, A. K. Molecular Transport Through Capillaries Made With Atomic-Scale Precision. *Nature* **2016**, *538*, 222−225.

(7) Tunuguntla, R. H.; Henley, R. Y.; Yao, Y.-C.; Pham, T. A.; Wanunu, M.; Noy, A. Enhanced Water Permeability and Tunable Ion Selectivity in Subnanometer Carbon Nanotube Porins. *Science* **2017**, *357*, 792−796.

(8) Zhang, S. Fabrication of Novel Biomaterials Through Molecular Self-Assembly. *Nat. Biotechnol.* **2003**, *21*, 1171−1178.

(9) Li, H.; Eddaoudi, M.; O'Keeffe, M.; Yaghi, O. M. Design and Synthesis of an Exceptionally Stable and Highly Porous Metal-Organic Framework. *Nature* **1999**, *402*, 276−279.

(10) Lee, J. Y.; Farha, O. K.; Roberts, J.; Scheidt, K. A.; Nguyen, S. B. T.; Hupp, J. T. Metal Organic Framework Materials as Catalysts. *Chem. Soc. Rev.* **2009**, *38*, 1450−1459.

(11) Côté, A. P.; Benin, A. I.; Ockwig, N. W.; O'Keeffe, M.; Matzger, A. J.; Yaghi, O. M. Porous, Crystalline, Covalent Organic Frameworks. *Science* **2005**, *310*, 1166−1170.

(12) Ding, S.-Y.; Gao, J.; Wang, Q.; Zhang, Y.; Song, W.-G.; Su, C.-Y.; Wang, W. Construction of Covalent Organic Framework for Catalysis: Pd/COF-LZU1 in Suzuki-Miyaura Coupling Reaction. *J. Am. Chem. Soc.* **2011**, *133*, 19816−19822.

(13) Khazanovich, N.; Granja, J. R.; McRee, D. E.; Milligan, R. A.; Ghadiri, M. R. Nanoscale Tubular Ensembles with Specified Internal Diameters. Design of a Self-Assembled Nanotube with a 13-Å Pore. *J. Am. Chem. Soc.* **1994**, *116*, 6011−6012.

(14) Hong, B. H.; Lee, J. Y.; Lee, C.-W.; Kim, J. C.; Bae, S. C.; Kim, K. S. Self-Assembled Arrays of Organic Nanotubes with Infinitely Long One-Dimensional H-Bond Chains. *J. Am. Chem. Soc.* **2001**, *123*, 10748−10749.

(15) Shimizu, L. S.; Smith, M. D.; Hughes, A. D.; Shimizu, K. D. Self-Assembly of a Bis-Urea Macrocycle Into a Columnar Nanotube. *Chem. Commun.* **2001**, *0*, 1592−1593.

(16) Jasti, R.; Bhattacharjee, J.; Neaton, J. B.; Bertozzi, C. R. Synthesis, Characterization, and Theory of [9]-, [12]-, and [18]-Cycloparaphenylene: Carbon Nanohoop Structures. *J. Am. Chem. Soc.* **2008**, *130*, 17646−17647.

(17) Darzi, E. R.; Sisto, T. J.; Jasti, R. Selective Syntheses of [7]-[12]Cycloparaphenylenes Using Orthogonal Suzuki-Miyaura Cross-Coupling Reactions. *J. Org. Chem.* **2012**, *77*, 6624−6628.
(18) Xia, J.; Jasti, R. Synthesis, Characterization, and Crystal Structure of [6]Cycloparaphenylene. *Angew. Chem., Int. Ed.* **2012**, *51*, 2474−2476.
(19) Patel, V. K.; Kayahara, E.; Yamago, S. Practical Synthesis of [*n*]Cycloparaphenylenes (*n* = 5, 7−12) by H_2SnCl_4 Mediated Aromatization of 1,4 Dihydroxycyclo 2,5 diene Precursors. *Chem. - Eur. J.* **2015**, *21*, 5742−5749.
(20) Evans, P. J.; Darzi, E. R.; Jasti, R. Efficient Room-Temperature Synthesis of a Highly Strained Carbon Nanohoop Fragment of Buckminsterfullerene. *Nat. Chem.* **2014**, *6*, 404−408.
(21) Ball, M.; Fowler, B.; Li, P.; Joyce, L. A.; Li, F.; Liu, T.; Paley, D.; Zhong, Y.; Li, H.; Xiao, S.; Ng, F.; Steigerwald, M. L.; Nuckolls, C. Chiral Conjugated Corrals. *J. Am. Chem. Soc.* **2015**, *137*, 9982−9987.
(22) Povie, G.; Segawa, Y.; Nishihara, T.; Miyauchi, Y.; Itami, K. Synthesis of a Carbon Nanobelt. *Science* **2017**, *356*, 172−175.
(23) Darzi, E. R.; Jasti, R. The Dynamic, Size-Dependent Properties of [5]-[12]Cycloparaphenylenes. *Chem. Soc. Rev.* **2015**, *44*, 6401−6410.
(24) Segawa, Y.; Miyamoto, S.; Omachi, H.; Matsuura, S.; Šenel, P.; Sasamori, T.; Tokitoh, N.; Itami, K. Concise Synthesis and Crystal Structure of [12]Cycloparaphenylene. *Angew. Chem., Int. Ed.* **2011**, *50*, 3244−3248.
(25) Leonhardt, E. J.; Van Raden, J. M.; Miller, D.; Zakharov, L. N.; Alemán, B.; Jasti, R. A Botton-Up Approach to Solution-Processed, Atomically Precise Graphitic Cylinders on Graphite. *Nano Lett.* **2018**, *18*, 7991−7997.
(26) Patrick, C. R.; Prosser, G. S. A Molecular Complex of Benzene and Hexafluorobenzene. *Nature* **1960**, *187*, 1021.
(27) Thalladi, V. R.; Weiss, H.-C.; Bläser, D.; Boese, R.; Nangia, A.; Desiraju, G. R. C-H···F Interactions in the Crystal Structures of Some Fluorobenzenes. *J. Am. Chem. Soc.* **1998**, *120*, 8702−8710.
(28) Hashimoto, S.; Kayahara, E.; Mizuhata, Y.; Tokitoh, N.; Takeuchi, K.; Ozawa, F.; Yamago, S. Synthesis and Physical Properties of Polyfluorinated Cycloparaphenylenes. *Org. Lett.* **2018**, *20*, 5973−5976.
(29) Schwaben, J.; Münster, N.; Breuer, T.; Klues, M.; Harms, K.; Witte, G.; Koert, U. Synthesis and Solid State Structures of 6,13 Bis(trifluoromethyl) and 6,13 Dialkoxypentacene. *Eur. J. Org. Chem.* **2013**, *2013*, 1639−1643.
(30) Bezdek, A.; Kuperberg, W. Maximum Density Space Packing with Congruent Circular Cylinders of Infinite Length. *Mathematika* **1990**, *37*, 74−80.
(31) Coates, G. W.; Dunn, A. R.; Henling, L. M.; Dougherty, D. A.; Grubbs, R. H. Phenyl-Perfluorophenyl Stacking Interactions: A New Strategy for Supermolecule Construction. *Angew. Chem., Int. Ed. Engl.* **1997**, *36*, 248−251.
(32) Kissel, P.; Murray, D. J.; Wulftange, W. J.; Catalano, V. J.; King, B. T. A Nanoporous Two-Dimensional Polymer by Single-Crystal-to-Single-Crystal Photopolymerization. *Nat. Chem.* **2014**, *6*, 774−778.
(33) Kayahara, E.; Sakamoto, Y.; Suzuki, T.; Yamago, S. Selective Synthesis and Crystal Structure of [10]Cycloparaphenylene. *Org. Lett.* **2012**, *14*, 3284−3287.
(34) Xia, J.; Bacon, J. W.; Jasti, R. Gram-Scale Synthesis and Crystal Structures of [8]- and [10]CPP, and the Solid-State Structure of C_{60}@[10]CPP. *Chem. Sci.* **2012**, *3*, 3018−3021.
(35) Koga, K.; Gao, G. T.; Tanaka, H.; Zeng, X. C. Formation of Ordered Ice Nanotubes Inside Carbon Nanotubes. *Nature* **2001**, *412*, 802−805.
(36) Hornbaker, D. J.; Kahng, S.-J.; Misra, S.; Smith, B. W.; Johnson, A. T.; Mele, E. J.; Luzzi, D. E.; Yazdani, A. Mapping the One-Dimensional Electronic States of Nanotube Peapod Structures. *Science* **2002**, *295*, 828−831.
(37) Chuvilin, A.; Bichoutskaia, E.; Gimenez-Lopez, M. C.; Chamberlain, T. W.; Rance, G. A.; Kuganathan, N.; Biskupek, J.; Kaiser, U.; Khlobystov, A. N. Self-Assembly of a Sulphur-Terminated Graphene Nanoribbon Within a Single-Walled Carbon Nanotube. *Nat. Mater.* **2011**, *10*, 687−692.
(38) Iwamoto, T.; Watanabe, Y.; Sadahiro, T.; Haino, T.; Yamago, S. Size Selective Encapsulation of C_{60} by [10]Cycloparaphenylene: Formation of the Shortest Fullerene Peapod. *Angew. Chem., Int. Ed.* **2011**, *50*, 8342−8344.
(39) Sato, S.; Yamasaki, T.; Isobe, H. Solid-State Structures of Peapod Bearings Composed of Finite Single-Wall Carbon Nanotube and Fullerene Molecules. *Proc. Natl. Acad. Sci. U. S. A.* **2014**, *111*, 8374−8379.
(40) Xu, Y.; Wang, B.; Kaur, R.; Minameyer, M. B.; Bothe, M.; Drewello, T.; Guldi, D. M.; von Delius, M. A Supramolecular [10]CPP Junction Enables Efficient Electron Transfer in Modular Porphyrin-[10]CPP⊃Fullerene Complexes. *Angew. Chem., Int. Ed.* **2018**, *57*, 11549−11553.
(41) Xu, Y.; Kaur, R.; Wang, B.; Minameyer, M. B.; Gsänger, S.; Meyer, B.; Drewello, T.; Guldi, D. M.; von Delius, M. Concave-Convex *π*-*π* Template Approach Enables the Synthesis of [10]-Cycloparaphenylene-Fullerene [2]Rotaxanes. *J. Am. Chem. Soc.* **2018**, *140*, 13413−13420.
(42) Iwamoto, T.; Slanina, Z.; Mizorogi, N.; Guo, J.; Akasaka, T.; Nagase, S.; Takaya, H.; Yasuda, N.; Kato, T.; Yamago, S. Partial Charge Transfer in the Shortest Possible Metallofullerene Peapod, La@C_{82}⊂[11]Cycloparaphenylene. *Chem. - Eur. J.* **2014**, *20*, 14403−14409.
(43) Ueno, H.; Nishihara, T.; Segawa, Y.; Itami, K. Cycloparaphenylene-Based Ionic Donor-Acceptor Supramolecule: Isolation and Characterization of Li^+@C_{60}⊂[10]CPP. *Angew. Chem., Int. Ed.* **2015**, *54*, 3707−3711.
(44) Britz, D. A.; Khlobystov, A. N.; Porfyrakis, K.; Ardavan, A.; Briggs, G. A. D. Chemical Reactions Inside Single-Walled Carbon Nano Test-Tubes. *Chem. Commun.* **2005**, *0*, 37−39.
(45) Barnes, J. C.; Dale, E. J.; Prokofjevs, A.; Narayanan, A.; Gibbs-Hall, I. C.; Juríček, M.; Stern, C. L.; Sarjeant, A. A.; Botros, Y. Y.; Stupp, S. I.; Stoddart, J. F. Semiconducting Single Crystals Comprising Segregated Arrays of Complexes of C_{60}. *J. Am. Chem. Soc.* **2015**, *137*, 2392−2399.
(46) Cooper, A. I. Porous Molecular Solids and Liquids. *ACS Cent. Sci.* **2017**, *3*, 544−553.
(47) Ding, S.-Y.; Wang, W. Covalent Organic Frameworks (COFs): From Design to Applications. *Chem. Soc. Rev.* **2013**, *42*, 548−568.
(48) Waller, P. J.; Gandara, F.; Yaghi, O. M. Chemistry of Covalent Organic Frameworks. *Acc. Chem. Res.* **2015**, *48*, 3053−3063.
(49) Furukawa, H.; Cordova, K. E.; O'Keefe, M.; Yaghi, O. M. The Chemistry and Applications of Metal-Organic Frameworks. *Science* **2013**, *341*, 1230444.
(50) Cui, Y.; Li, B.; He, H.; Zhou, W.; Chen, B.; Qian, G. Metal-Organic Frameworks as Platforms for Functional Materials. *Acc. Chem. Res.* **2016**, *49*, 483−493.
(51) Lim, S.; Kim, H.; Selvapalam, N.; Kim, K.; Cho, S. J.; Seo, G.; Kim, K. Cucurbit[6]uril: Organic Molecular Porous Material with Permanent Porosity, Exceptional Stability, and Acetylene Sorption Properties. *Angew. Chem., Int. Ed.* **2008**, *47*, 3352−3355.
(52) Dewal, M.; Xu, Y.; Yang, J.; Mohammed, F.; Smith, M.; Shimizu, L. Manipulating the Cavity of a Porous Material Changes the Photoreactivity of Included Guests. *Chem. Commun.* **2008**, *33*, 3909−3911.
(53) Tan, L.; Li, H.; Tao, Y.; Zhang, S. X.; Wang, B.; Yang, Y. Pillar[5]arene-Based SOF for Highly Selective CO_2-Capture at Ambient Conditions. *Adv. Mater.* **2014**, *26*, 7027−7031.
(54) Sakamoto, H.; Fujimori, T.; Li, X.; Kaneko, K.; Kan, K.; Ozaki, N.; Hijikata, Y.; Irle, S.; Itami, K. Cycloparaphenylene as a Molecular Porous Carbon Solid with Uniform Pores Exhibiting Absorption-Induced Softness. *Chem. Sci.* **2016**, *7*, 4204−4210.
(55) Webb, P. A.; Orr, C. *Analytical Methods in Fine Particle Technology*; Micromeritics Instrument Corp.: 1997.
(56) Reche-Tamayo, M.; Moral, M.; Pérez-Jiménez, A. J.; Sancho-García, J. C. Theoretical Determination of Interaction and Cohesive

DOI: 10.1021/acs.joc.9b02340
J. Org. Chem. 2020, 85, 129−141

Energies of Weakly Bound Cycloparaphenylene Molecules. *J. Phys. Chem. C* **2016**, *120*, 22627−22634.
(57) Grimme, S.; Antony, J.; Ehrlich, S.; Krieg, H. A Consistent and Accurate Ab Initio Parameterization of Density Functional Dispersion Correction (DFT-D) for the 94 Elements H-Pu. *J. Chem. Phys.* **2010**, *132*, 154104.
(58) Grimme, S.; Ehrlich, S.; Goerigk, L. Effect of the Damping Function in Dispersion Corrected Density Functional Theory. *J. Comput. Chem.* **2011**, *32*, 1456−1465.
(59) Becke, A. D. Density-Functional Thermochemistry. III. The Role of Exact Exchange. *J. Chem. Phys.* **1993**, *98*, 5648−5652.
(60) Frisch, M. J.; Trucks, G. W.; Schlegel, H. B.; Scuseria, G. E.; Robb, M. A.; Cheeseman, J. R.; Scalmani, G.; Barone, V.; Petersson, G. A.; Nakatsuji, H.; Li, X.; Caricato, M.; Marenich, A.; Bloino, J.; Janesko, B. G.; Gomperts, R.; Mennucci, B.; Hratchian, H. P.; Ortiz, J. V.; Izmaylov, A. F.; Sonnenberg, J. L.; Williams-Young, D.; Ding, F.; Lipparini, F.; Egidi, F.; Goings, J.; Peng, B.; Petrone, A.; Henderson, T.; Ranasinghe, D.; Zakrzewski, V. G.; Gao, J.; Rega, N.; Zheng, G.; Liang, W.; Hada, M.; Ehara, M.; Toyota, K.; Fukuda, R.; Hasegawa, J.; Ishida, M.; Nakajima, T.; Honda, Y.; Kitao, O.; Nakai, H.; Vreven, T.; Throssell, K.; Montgomery, J. A., Jr.; Peralta, J. E.; Ogliaro, F.; Bearpark, M.; Heyd, J. J.; Brothers, E.; Kudin, K. N.; Staroverov, V. N.; Keith, T.; Kobayashi, R.; Normand, J.; Raghavachari, K.; Rendell, A.; Burant, J. C.; Iyengar, S. S.; Tomasi, J.; Cossi, M.; Millam, J. M.; Klene, M.; Adamo, C.; Cammi, R.; Ochterski, J. W.; Martin, R. L.; Morokuma, K.; Farkas, O.; Foresman, J. B.; Fox, D. J. *Gaussian 09*, Revision D.01; Gaussian, Inc.: Wallingford, CT, 2016.
(61) Battaglia, M. R.; Buckingham, A. D.; Williams, J. H. The Electric Quadrupole Moments of Benzene and Hexafluorobenzene. *Chem. Phys. Lett.* **1981**, *78*, 421−423.
(62) Shimizu, K.; Costa Gomes, M. F.; Pádua, A. A. H.; Rebelo, L. P. N.; Lopes, J. N. C. On the Role of the Dipole and Quadrupole Moments of Aromatic Compounds in the Solvation by Ionic Liquids. *J. Phys. Chem. B* **2009**, *113*, 9894−9900.
(63) Martinez, C. R.; Iverson, B. L. Rethinking the Term "Pi-Stacking. *Chem. Sci.* **2012**, *3*, 2191−2201.
(64) Lovell, T. C.; Colwell, C. E.; Zakharov, L. N.; Jasti, R. Symmetry Breaking and the Turn-On Fluorescence of Small, Highly Strained Carbon Nanohoops. *Chem. Sci.* **2019**, *10*, 3786−3790.
(65) Black, C. B.; Andrioletti, B.; Try, A. C.; Ruiperez, C.; Sessler, J. L. Dipyrrolylquinoxalines: Efficient Sensors for Fluoride Anion in Organic Solution. *J. Am. Chem. Soc.* **1999**, *121*, 10438−10439.
(66) Sheldrick, G. M. *Bruker/Siemens Area Detector Absorption Correction Program*; Bruker AXS: Madison, WI, 1998.
(67) Sheldrick, G. M. Crystal Structure Refinement with SHELXL. *Acta Crystallogr., Sect. C: Struct. Chem.* **2015**, *C71*, 3−8.
(68) Van der Sluis, P.; Spek, A. L. BYPASS: An Effective Method for the Refinement of Crystal Structures Containing Disordered Solvent Regions. *Acta Crystallogr., Sect. A: Found. Crystallogr.* **1990**, *A46*, 194−201.
(69) Rouquerol, J.; Llewellyn, P.; Rouquerol, F. *Stud. Surf. Sci. Catal.* **2007**, *160*, 49−56.

DOI: 10.1021/acs.joc.9b02340
J. Org. Chem. 2020, 85, 129−141